Experimental Investigation of Parametric Transfer in Synchronously Pumped Optical Parametric Oscillators

Hazel S.S. Hung, Jerry Prawiharjo, Nikita K. Daga, David C. Hanna, David P. Shepherd

Optoelectronics Research Centre, University of Southampton, Southampton, S017 1BJ, UK

We experimentally investigate the parameters affecting parametric transfer in a SPOPO for indirect shaping of MIR ultrashort pulses and make comparisons with previously reported numerical modeling. The individual effects of the parameters are discussed in detail. We conclude that signal bandwidth narrowing, minimal signal amplification, large pump depletion, cavity length tuning and minimal pump and idler temporal walk-off are required for high fidelity transfer, which we are able to demonstrate for a strongly chirped pump pulse.

OCIS codes: 190.4410, 190.4970, 320.5540, 320.7110.

1. Introduction

Tailoring ultrashort pulses in the mid-infrared wavelength regime is a powerful technique for applications in spectroscopy [1–3] and particularly coherent control [4–7], where having adaptive control over the pulse shape can significantly enhance the outcome of chemical reactions.

Many of the commercially available pulse shaping devices such as liquid crystal modulators (LCMs) [8] and acousto-optic modulators (AOMs) are normally only suitable for the visible and near-infrared (NIR) wavelengths, requiring that alternative methods be used for other regimes such as the ultraviolet (UV) or mid-infrared (MIR). Such methods include the use of a micromirror array for phase-only pulse shaping [9] as well as spectral amplitude and phase shaping with a fused silica AOM [10] for the UV. Direct shaping of MIR pulses has been demonstrated with dispersive fibres and/or grating compressors [11–13] but these techniques are not programmable and therefore not suited to adaptive pulse shaping. More recently however, high resolution pulse shaping was achieved using a Ge-doped AOM [14] but such acoustic devices are limited to kilohertz repetition rates.

An alternative approach is to indirectly shape the pulse by initial shaping in the NIR before transferring the pulse to the MIR using an optical parametric process. Such a method was initially demonstrated with difference frequency generation (DFG) from the leading and trailing spectral edges of a chirped femtosecond pulse [15, 16]

generating wavelengths beyond 10μm. However other schemes have demonstrated greater wavelength tunability and higher pulse energies from DFG of a spectrally narrow pulse and a highly complex pulse generating shaped MIR pulses [1, 17].

Previously, we have demonstrated adaptive pulse shaping in the MIR using a synchronously pumped optical parametric oscillator (SPOPO) achieving both compression and the generation of a MIR double pulse output from an originally chirped NIR pump pulse [18]. Following this demonstration of the potential for this adaptive MIR pulse shaping technique, we progressed to numerical studies of the fidelity of transfer, firstly in the simple single pass DFG process [19] and then to the somewhat more complicated case of the SPOPO [20]. The effects of temporal walk-off (TWO), group delay dispersion (GDD), signal bandwidth, signal amplification and pump depletion were considered. We found that good fidelity of transfer to the idler could be achieved by ensuring high pump depletion, low signal amplification, a narrow signal bandwidth, minimising the pump and idler TWO and GDD, and compensating for the pump and signal TWO by cavity length tuning.

In this paper, we experimentally investigate the parameters that affect parametric transfer in a SPOPO, based on the findings from the previous theoretical work [20]. To the best of our knowledge, this is the first experimental study of parametric transfer in a SPOPO and by collective consideration of all investigated factors we demonstrate high fidelity transfer to the MIR idler pulse. In section 2 the experimental arrangement of the SPOPO and pulse characterization are described. Results for experiments

investigating the factors affecting parametric transfer are shown in section 3. Finally, we conclude in section 4 with a discussion of our results.

2. Experimental Arrangement

A schematic representation of the SPOPO setup is shown in Fig.1. The SPOPO comprises of a resonator of four mirrors arranged in a bow-tie configuration, a periodically poled lithium niobate (PPLN) crystal as the nonlinear medium, and an etalon for spectrally narrowing the signal pulse. The mirrors are highly reflecting at $\sim 1200 - 2000\,\mathrm{nm}$, though a small amount of the signal is detected through M4 for SPOPO monitoring purposes. Two curved mirrors (CM1,CM2) are used to achieve a near confocal focusing condition for the resonating signal pulse over the crystal length for optimum gain. The overall resonator length is set such that the signal round-trip time is comparable to the pump repetition period.

Our continuous pump pulse train was generated by a Nd:YLF laser/amplifier system, which was then spectrally broadened via self phase modulation (SPM) in a polarization-maintaining single-mode fibre. This delivers a train of pulses into the SPOPO at a repetition rate of 120 MHz, each with a 4 ps pulse-width at a central wavelength of 1047 nm and a spectral FWHM of $\sim 3.5\,\mathrm{nm}$ (958 GHz), with an average power of up to 1.15 W. It should be noted that the operation of this system varied slightly from day to day, resulting in a small variation of the spectral intensity profile in our different experiments.

The 10.7 mm long PPLN crystal was operated at a fixed temperature of 110°C and had five different poling periods ranging from 29.2 μm to 30.2 μm to allow signal wavelengths between 1480 nm and 1600 nm to be obtained, corresponding to an idler wavelength range of 3580 nm to 3030 nm. These parameters are summarized in Fig. 2(a). The Sellmeier equation [21] was used to estimate the group velocity and its dispersion parameter (GVD) for the interacting pulses in lithium niobate. The calculated TWO between the pump and idler pulses and that between the pump and signal pulses for the wavelengths used in our experiment are given in Fig. 2(b). It can be seen that minimum pump-idler TWO occurs at signal and idler wavelengths of 1505 and 3440 nm, respectively. For our pump pulse parameters, we calculated that the effect of the GDD in the lithium niobate can be neglected.

Complete characterization of the pump and idler pulses was achieved using the cross-correlation sonogram technique [22], schematically depicted in Fig. 3. The setup consists of a temporal delay arm and a spectral gating arm arranged in a zero dispersion configuration. Two-photon absorption (TPA) cross-correlations between the temporally delayed and spectrally filtered pulses were taken at discrete frequencies to build sonogram traces, from which the spectral phase and amplitude of the input pulse were retrieved with an iterative deconvolution algorithm. A full sonogram trace made of fifty discrete frequencies was acquired in less than four minutes. Characterization of the pump and idler pulses used similar setups but with one of the major differences being the use of different detectors, a GaAsP detector for the NIR and an

extended InGaAs detector for the MIR. In both cases, the spectral gating arm employed a slit of width one-tenth of the total spectral width. Furthermore, we employed a phase-sensitive detection scheme using a lock-in amplifier to improve the sensitivity of our setup. A measured and retrieved sonogram trace together with the retrieved spectral phase and intensity, and the autocorrelation of a typical input pump pulse are shown in Fig. 4.

3. Results

In this section, we present our investigations on the effects of various SPOPO parameters on the parametric transfer. We cover the effect of parameters such as etalon thickness, input pump power and signal amplification. In addition, the effects of chromatic dispersion, specifically the TWO between the interacting pulses, are investigated.

In analyzing the transfer fidelity, we compared the autocorrelations, spectral intensities, and sonograms of the pump and idler. However, we will mainly show the comparison between the pump and idler spectra since, for many of the results, it was found that the autocorrelations and spectral phases showed similar profiles, and that much of the change was in the frequency domain. We have therefore chosen a quantitative measure of the fidelity based on spectral intensity via the following overlap relation:

$$z = 1 - \frac{\int \left|\widetilde{E}_p(\Omega)\right|^2 \left|\widetilde{E}_i(\Omega)\right|^2 d\Omega}{\left[\int \left|\widetilde{E}_p(\Omega)\right|^4 d\Omega \int \left|\widetilde{E}_i(\Omega)\right|^4 d\Omega\right]^{1/2}}, \tag{1}$$

where Ω is the frequency detuning and $\left|\widetilde{E}_{p,i}(\Omega)\right|^2$ is the spectral intensity of the pump or idler, as denoted by the subscripts p and i, respectively. This equation is analogous to the expression for Z given in Ref. [20], comparing the overlap of the pump and idler spectrograms. As with Z, the spectral transfer fidelity z, ranges between zero and unity, where zero corresponds to perfect overlap and unity indicates no overlap.

From our numerical investigations [20], we identified parameters leading to a high fidelity parametric transfer, such as, placing an optical band-pass filter in the resonator, working at high pump depletion and low signal amplification, tuning the cavity length to compensate for the pump-signal TWO, and selecting the appropriate crystal length or idler wavelength to minimise pump-idler TWO. We therefore complied with these requirements by providing the cavity with an etalon whilst maintaining a low loss cavity by using mirrors that are highly reflecting at the signal wavelengths, working with a pump power at three times above threshold to achieve significant pump depletion whilst avoiding the back-conversion regime, and choosing the idler wavelength to be 3440 nm. Our subsequent investigations were based on altering individual parameters around this operating condition.

3.A. Resonator Parameters and Process Nonlinearity

Operating the SPOPO using the standard configuration described in the previous section, we start by investigating the effect of the etalon on the signal bandwidth and on the transfer fidelity. Without an etalon in the cavity, we measured the signal bandwidth at 1505 nm to be 1.3 nm (172 GHz), and the threshold was ∼100 mW. We then placed an etalon in the resonator observing an increase in theshold due to the losses induced by the etalon. We used two etalons of different thicknesses, resulting in signal bandwidths, measured with a resolution of 0.1 nm, of 0.5 and 0.8 nm (66 and 106 GHz), and both with similar thresholds at 180mW. The etalon angle was adjusted to ensure that the centre wavelength of the resonating signal pulse was the same in all cases. In addition, all results were taken operating at three times above threshold. A small adjustment of the cavity length was made to symmetrize the spectral transfer such that the two main idler spectral peaks were of the same height, as is the case for the pump spectrum (see Fig.4). Figure 5 shows the retrieved idler sonogram data for signal bandwidths of 1.3, 0.8, and 0.5 nm, corresponding to $z = 0.069, 0.020$, and 0.012, respectively. These results clearly show a significant improvement in fidelity of transfer when an etalon is placed within the resonator. Moreover, further narrowing of the signal bandwidth results in a better transfer of the two central peaks of the spectrum, a consequence of the convolution relation.

We next consider the effect of the pump depletion on the transfer fidelity. According

to our numerical investigations [20], higher pump depletion without going to the back-conversion regime results in an improvement of the transfer fidelity, except in the presence of GDD. The improvement of transfer fidelity with pump depletion is due to an effective temporal broadening of the signal pulse relative to the pump when considering a single pass DFG process. A more detailed explanation of this mechanism is given Ref. [19]. We find that our experimental SPOPO results agree with these numerical predictions. Figure 6 shows the idler spectra for pump power ranging from two to six times above the threshold of 180 mW. It can be easily seen that, in addition to the variation in the symmetry of the idler spectra, the transfer resolution improves with increasing input power. The corresponding spectral transfer fidelity is plotted in Fig. 7(b) showing an optimum at an operation of around four times above threshold. This point roughly coincides with the maximum pump depletion shown in Fig. 7(a), which is in agreement with the numerical investigations for negligible GDD.

The final resonator parameter we investigated was the resonator loss by replacing mirror M4 from Fig. 1 with mirrors of different signal reflectivities. Our numerical investigations found that increasing the resonator loss and hence increasing the required signal gain worsens the transfer fidelity as is predicted by the single pass DFG process [19]. Moreover, we have observed both theoretically [20] and experimentally that a high resonator loss reduces the effect of the etalon as the signal bandwidth is broader at steady state. We operated our SPOPO using the standard configuration at two-and-a-half times above the threshold in this investigation, due to the

maximum available pump power. The resulting idler spectra for M4 reflectivities of 65%, 85% and 100%, corresponding to $z = 0.040, 0.017$ and 0.014, respectively, are shown in Fig. 8. It can be clearly observed that the fidelity improves with increasing M4 reflectivity, confirming our numerical investigations. The resolution of the central peaks also improves due to an associated narrowing of the signal spectrum but, unlike the results for increasing pump power, the overall symmetry of the spectra remain unchanged.

3.B. Chromatic Dispersion

Having investigated the effects of the resonator parameters, we now study the effects of the PPLN chromatic dispersion on the parametric transfer. More specifically, we investigate the effect of the TWO between the interacting pulses, since the effect of the GDD is negligible for our experimental configuration.

We start by investigating the effect of the pump-signal TWO. For the combination of wavelengths we are working at, the signal group velocity is greater than the pump group velocity, causing the signal to walk through the pump in the PPLN and thus distorting the parametric transfer. In our numerical work [20], we have established that this effect can be compensated for by adjusting the cavity length in such a way that the signal arrives at the crystal after the pump pulse. Note that, in this paper, we define zero round-trip mismatch to correspond to the resonator length at which minimum threshold is achieved. This is different from the definition in Ref. [20] that

corresponds to the length for which the pump and signal pulse peaks enter the crystal at the same time. Hence, the two definitions are related by some temporal offset which has not been experimentally determined.

For this investigation, we used our standard SPOPO configuration, where the pump-idler TWO was ∼48 fs, and consequently the pump-signal TWO at ∼1 ps. We used an etalon to restrict the signal bandwidth to ∼100 GHz at a centre wavelength of 1505 nm. Figure 9 shows the measured idler spectra for cavity length detunings of $\pm 80\,\mu$m, $\pm 40\,\mu$m and $0\,\mu$m, corresponding to round-trip mismatches of ±267 fs, ±133 fs and 0 fs, respectively. An increase in cavity length detuning causes a delay in the signal pulse arrival at the PPLN entrance, causing the higher frequency spectral peak of the pump pulse, that corresponds to the trailing edge, to be transferred more efficiently. Note that at zero round-trip mismatch, the heights of the two larger spectral peaks are not quite equal as they are in the pump. Symmetric transfer to the idler occurs between a round-trip mismatch of zero and −133 fs, although this seems to be coupled with a slight degradation in fidelity of the center peaks of the spectrum. Conversely, decreasing the cavity length seems to improve the resolution of the central peaks but compromises the symmetry of the spectral transfer.

Having investigated the pump-signal TWO, we now investigate the effect of the pump-idler TWO. In this investigation, we changed the pump-idler TWO by varying the idler wavelength, which was achieved by using different QPM grating periods in our PPLN. As in previous investigations, we operated the SPOPO at three

times above threshold and used an etalon to narrow the signal spectral FWHM to ∼100 GHz. Figure 10 shows the idler spectra for five different PPLN poling periods, whose transfer fidelity z is plotted in Fig. 11. It can be easily seen that the best fidelity is achieved at minimum pump-idler TWO where the working idler wavelength is 3440 nm. As the pump-idler TWO becomes more positive, as shown in Fig. 10(c)-(e), the transfer fidelity of the lower frequency peak worsens. Similarly, as the pump-idler TWO becomes more negative, the transfer of the higher frequency peak is degraded, as shown Fig. 10(a).

It is important to mention that the degradation of the transfer fidelity indicated by the difference in the height of the two main spectral peaks cannot always be rectified by tuning the cavity length. When the SPOPO had a signal central wavelength of 1600 nm, we varied the cavity length by as much as $\pm 120\,\mu$m, corresponding to a total round-trip mismatch of ±400 fs, and obtained various idler spectra as shown in Fig. 12. It can be seen from this that increasing the lower frequency peak degrades the transfer of the middle spectral peaks with no improvement to the general fidelity of the pulse.

We compared the spectral fidelity z for our SPOPO working at two different wavelengths at various cavity length offsets in Fig. 13. For both cases, it can be observed that minimum z coincides with near maximum pump depletion. For λ_s =1600 nm, the maximum achievable pump depletion is lower than for λ_s = 1505 nm and the rate of change of depletion with cavity length detuning is faster. However, despite the

relatively small change in the pump depletion behavior, the spectral transfer fidelity is significantly worsened by the increase in pump-idler TWO. The general trends of pump depletion and fidelity described here are in good agreement with our numerical results [20].

3.C. High fidelity transfer

Finally, based on our investigations, we operated our SPOPO for high fidelity transfer by placing an etalon in the cavity to reduce the signal spectral FWHM to ∼80 GHz, choosing a PPLN grating with minimal pump-idler TWO working at $\lambda_i = 3440$ nm, compensating the pump-signal TWO by tuning the cavity length, using a low loss resonator and operating at four times above threshold to achieve a significant pump depletion. Figure 14(b) shows the retrieved idler sonogram trace obtained under these conditions looking almost identical to the retrieved pump sonogram trace in Fig. 14(a). Closer inspection of the pulses can be seen in Fig. 14(d) where comparison of the pump and idler spectra and phase show that they are in good agreement except for a small discrepancy in the middle peaks. Comparison to Fig. 14(c) and (e) where there is no signal bandwidth narrowing or cavity length tuning emphasizes the importance of implementing the measures that we have identfied for enhancing fidelity. Such implementation, in this case, has resulted in an order of magnitude improvement of spectral transfer from $z = 0.15$ to 0.015.

4. Conclusions

We have experimentally investigated the factors affecting parametric transfer from the pump to the idler in a SPOPO. The results presented here are in good agreement with the numerical predictions in previous work [20]. We have shown that signal bandwidth narrowing significantly improves the transfer and is easily achieved with an etalon in the SPOPO cavity. A low loss resonator achieved by the use of highly reflecting mirrors is required as this minimises the signal gain and helps to maintain a narrow signal bandwidth. In addition to this, operation should be near maximum pump depletion, corresponding to around four times above oscillation threshold, and below the level at which back-conversion begins to distort the transfer.

Although the optimum threshold position is already very close to optimum fidelity, cavity length tuning can somewhat improve the fidelity by compensating for pump-signal TWO. Temporal walk-off between the pump and idler causes significant degradation of transfer fidelity such that good fidelity can only be achieved within a small tolerance of the zero walk-off condition for this SPOPO arrangement, severely restricting the tunability. However, a larger wavelength range could easily be accessed with shorter crystal lengths or with a tunable pump source to minimise pump-idler TWO.

For the SPOPO arrangement described in this work, high fidelity transfer was achieved by implementing the measures identified for fidelity enhancement. The qual-

ity of transfer was evident in the comparison of the pump and idler sonogram traces and the retrieved spectral phase and amplitude of the pulses. To quantify the fidelity, we calculated an order of magnitude improvement in spectral transfer fidelity. This demonstration of high fidelity transfer in a SPOPO from the NIR to the MIR realises the concept of high resolution MIR pulse shaping, via an optical parametric oscillator device. Without active preservation of the pulse shape, the work presented here has shown that the resolution of the required MIR pulse is severely hindered, thereby compromising the degree of precision that is essential for applications such as coherent control of molecules.

Acknowledgment

This work was supported by EPSRC Instrument Grant EP/C009479/1. Hazel S. S. Hung acknowledges the support of an EPSRC studentship. The author would like to thank Professor Derryck Reid of Heriot Watt University for helpful discussions on the cross-correlation sonogram technique used in the work presented here.

H.S.S.Hung's e-mail address is hssh@orc.soton.ac.uk

References

1. H. S. Tan and W. S. Warren, "Mid infrared pulse shaping by optical parametric amplification and its application to optical free induction decay measurement," Opt. Express **11**, 1021–1028 (2003).

2. K. A. Tillman, R. R. J. Maier, D. T. Reid, and E. D. McNaghten, "Mid-infrared absorption spectroscopy of methane using a broadband femtosecond optical parametric oscillator based on aperiodically poled lithium niobate," J. Opt. A. Pure. Appl. Opt. **7**, S408–S414 (2005).

3. H. K. Nienhuys, S. Woutersen, R. A. van Santen, and H. J. Bakker, "Mechanism for vibrational relaxation in water investigated by femtosecond infrared spectroscopy," J. Chem. Phys. **111**, 1494–1500 (1999).

4. L. Windhorn, J. S. Yeston, T. Witte, W. Fuss, M. Motzkus, D. Proch, K. L. Kompa, and C. B. Moore, "Getting ahead of IVR: A demonstration of mid-infrared induced molecular dissociation on a sub-statistical time scale," J. Chem. Phys. **119**, 641–645 (2003).

5. D. J. Maas, D. I. Duncan, R. B. Vrijen, W. J. van der Zande, and L. D. Noordam, "Vibrational ladder climbing in NO by (sub)picosecond frequency-chirped infrared laser pulses," Chem. Phys. Lett. **290**, 75–80 (1998).

6. T. Witte, T. Hornung, L. Windhorn, D. Proch, R. de Vivie-Riedle, M. Motzkus, and K. L. Kompa, "Controlling molecular ground-state dissociation by optimizing vibrational ladder climbing," J. Chem. Phys. **118**, 2021–2024 (2003).

7. C. Meier and M. C. Heitz, "Laser control of vibrational excitation in carboxyhemoglobin: A quantum wave packet study," J. Chem. Phys. **123**, 161–172 (2005).

8. A. M. Weiner, "Femtosecond pulse shaping using spatial light modulators," Rev.

Sci. Instrum. **71**, 1929–1960 (2000).

9. M. Hacker, G. Stobrawa, R. Sauerbrey, T. Buckup, M. Motzkus, M. Wildenhain, and A. Gehner, "Micromirror SLM for femtosecond pulse shaping in the ultraviolet," Appl. Phys. B **76**, 711–714 (2003).

10. M. Roth, M. Mehendale, A. Bartelt, and H. Rabitz, "Acousto-optical shaping of ultraviolet femtosecond pulses," Appl. Phys. B **80**, 441–444 (2005).

11. V. D. Kleiman, S. M. Arrivo, J. S. Melinger, and E. J. Heilweil, "Controlling condensed-phase vibrational excitation with tailored infrared pulses," Chem. Phys. **233**, 207–216 (1998).

12. G. M. H. Knippels, A. F. G. Vandermeer, R. Mols, P. W. Vanamersfoort, R. B. Vrijen, D. J. Maas, and L. D. Noordam, "Generation of frequency-chirped pulses in the far-infrared by means of a subpicosecond free-electron laser and an external pulse shaper," Opt. Commun. **118**, 546–550 (1995).

13. R. Kaindl, M. Wurm, K. Reimann, P. Hamm, A. Weiner, and M. Woerner, "Generation, shaping, and characterization of intense femtosecond pulses tunable from 3 to 20 μm," J. Opt. Soc. Am. B **17**, 2086–2094 (2000).

14. S. H. Shim, D. B. Strasfeld, E. C. Fulmer, and M. T. Zanni, "Femtosecond pulse shaping directly in the mid-IR using acousto-optic modulation," Opt. Lett. **31**, 838–840 (2006).

15. F. Eickemeyer, R. A. Kaindl, M. Woerner, T. Elsaesser, and A. M. Weiner, "Con-

trolled shaping of ultrafast electric field transients in the mid-infrared spectral range," Opt. Lett. **25**, 1472–1474 (2000).

16. N. Belabas, J. Likforman, L. Canioni, B. Bousquet, and M. Joffre, "Coherent broadband pulse shaping in the mid infrared," Opt. Lett. **26**, 743–745 (2001).
17. T. Witte, K. Kompa, and M. Motzkus, "Femtosecond pulse shaping in the mid infrared by difference-frequency mixing," Appl. Phys. B **76**, 467–471 (2003).
18. N. A. Naz, H. S. S. Hung, M. V. O'Connor, D. C. Hanna, and D. P. Shepherd, "Adaptively shaped mid-infrared pulses from a synchronously pumped optical parametric oscillator," Opt. Express **13**, 8400–8405 (2005).
19. J. Prawiharjo, H. S. S. Hung, D. C. Hanna, and D. P. Shepherd, "Theoretical and numerical investigations of parametric transfer via difference-frequency generation for indirect mid-infrared pulse shaping," J. Opt. Soc. Am. B **24**, 895–905 (2007).
20. J. Prawiharjo, H. S. S. Hung, D. C. Hanna, and D. P. Shepherd, "Numerical investigations of parametric transfer in synchronously pumped optical parametric oscillators for indirect mid-infrared pulse shaping," J. Opt. Soc. Am. B, doc. ID 82028 (posted July 2007, in press) .
21. D. H. Jundt, "Temperature-dependent sellmeier equation for the index of refraction, $n_{(e)}$, in congruent lithium niobate," Opt. Lett. **22**, 1553–1555 (1997).
22. I. Cormack, W. Sibbett, and D. Reid, "Rapid measurement of ultrashort-pulse amplitude and phase from a two-photon absorption sonogram trace," J. Opt. Soc.

Am. B **18**, 1377–1382 (2001).

List of Figures

14 Demonstration of high fidelity parametric transfer. (a) Retrieved pump sonogram, (b) retrieved idler sonogram for actively preserving parametric transfer and (c) retrieved idler sonogram with no attempts to preserve transfer. (d) and (e) show the retrieved pump spectrum and phase (dashed curve) compared with the measured idler spectrum (circles) and retrieved idler spectrum and phase (solid) for the SPOPO arrangements maintaining and not maintaining high fidelity transfer. 35

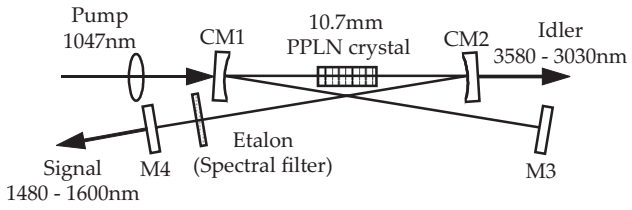

Fig. 1. Schematic arrangement of the SPOPO setup.

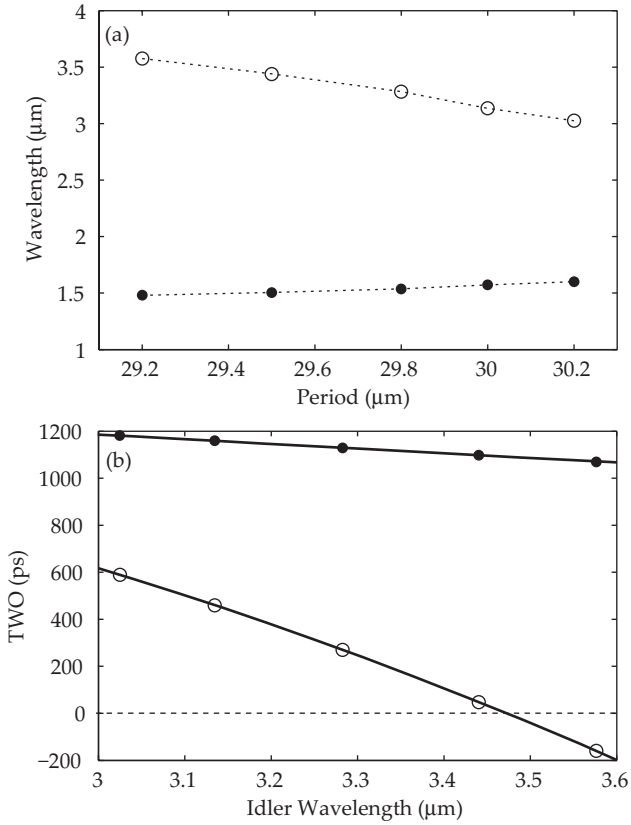

Fig. 2. (a) The SPOPO signal (solid circles) and idler (open circles) wavelengths corresponding to the 5 different poling periods used, (b) pump-idler TWO (solid circles) and pump-signal TWO (open circles) as a function of the idler wavelength for operation at 110°C. The data points correspond to the discrete idler wavelengths from the poling periods available.

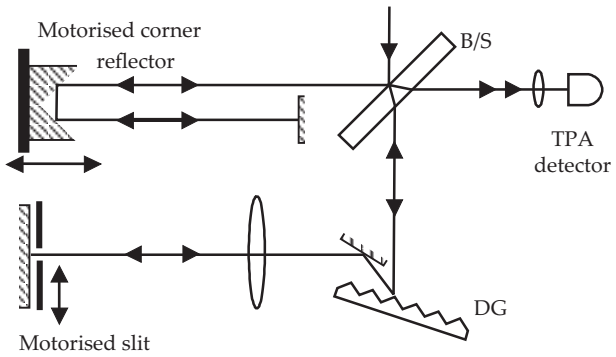

Fig. 3. Schematic arrangement of the cross-correlation sonogram setup.

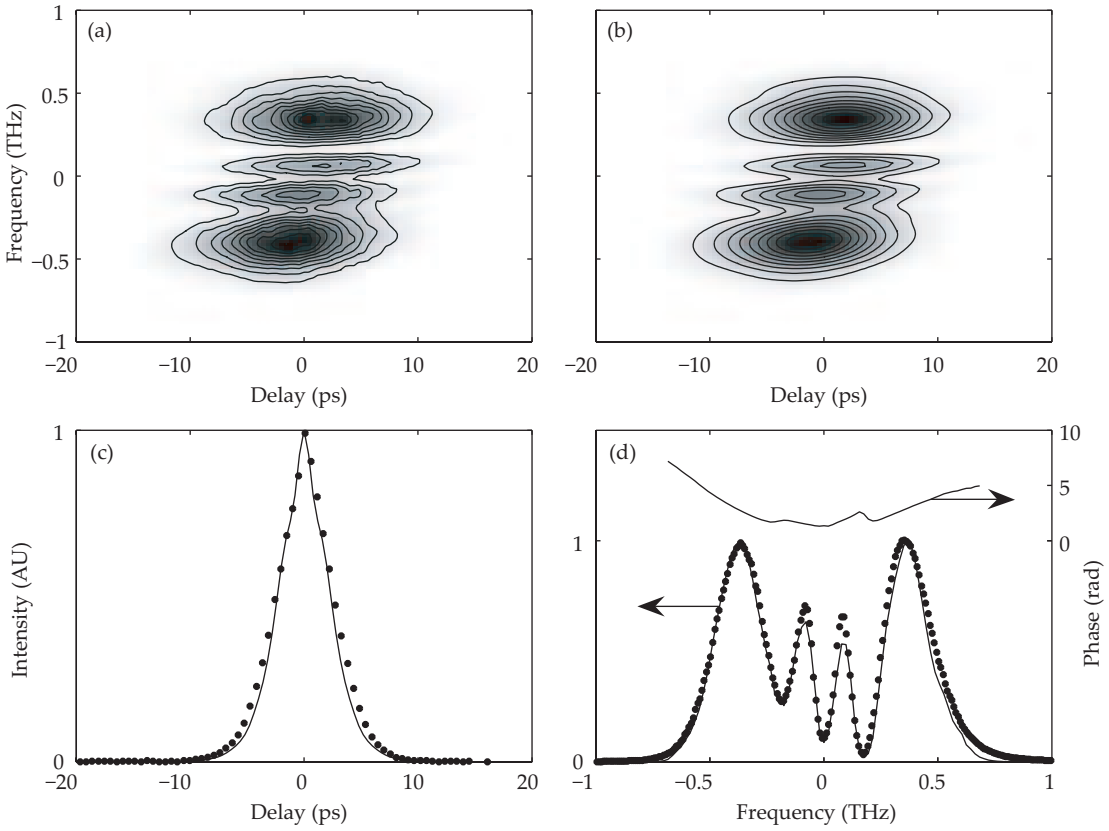

Fig. 4. Sonogram data of the input pump pulse: (a) measured sonogram, (b) retrieved sonogram, (c) measured (circles) and retrieved (solid curve) autocorrelation traces and (d) measured (circles) and retrieved (solid curve) spectra with the retrieved spectral phase.

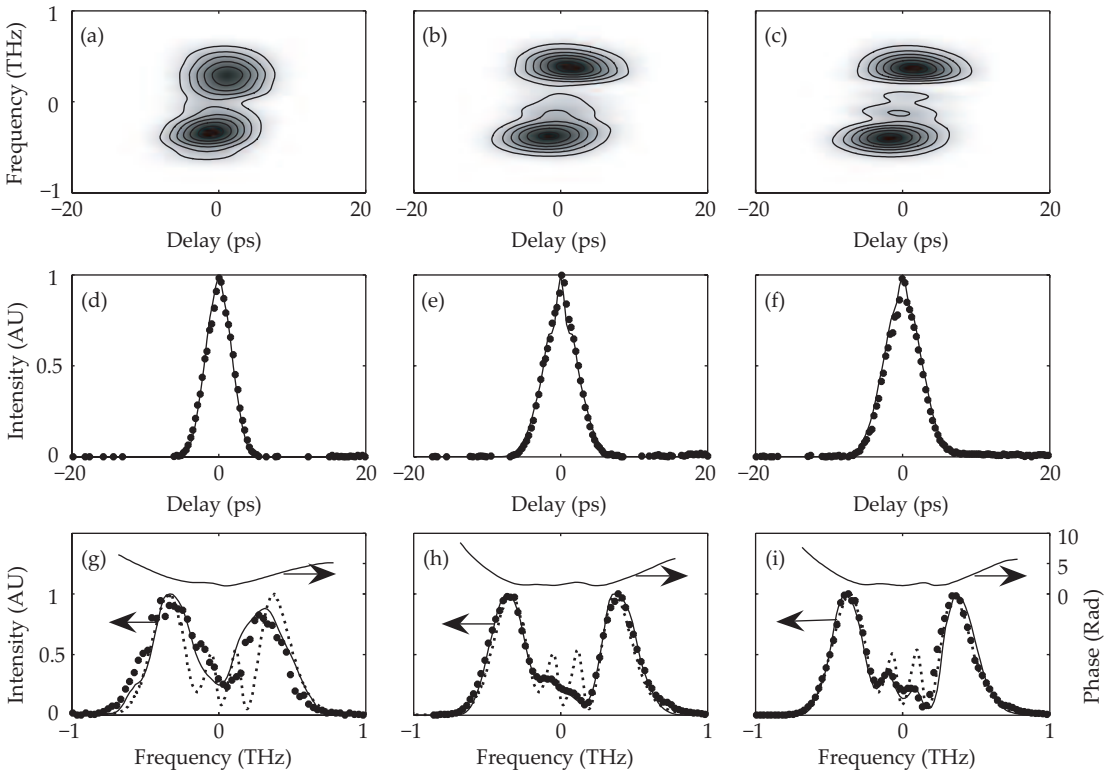

Fig. 5. Idler sonogram data for signal bandwidths of 1.3nm (first column), 0.8nm (second column) and 0.5nm (third column). (a)-(c) Retrieved sonograms, (d)-(f) measured (circles) and retrieved (solid curve) autocorrelations and (g)-(i) measured (circles) and retrieved (solid curve) spectra with the retrieved spectral phases (solid curve) and measured pump spectrum (dashed curve) for comparison.

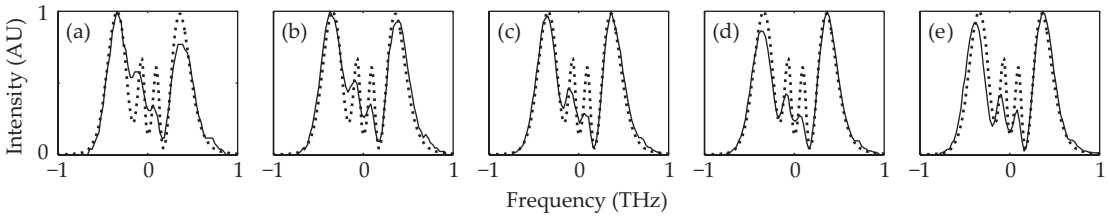

Fig. 6. Measured pump (dashed) and idler spectra (solid) for increasing input pump power at (a) 2×, (b) 3×, (c) 4×, (d) 5× and (e) 6× above oscillation threshold.

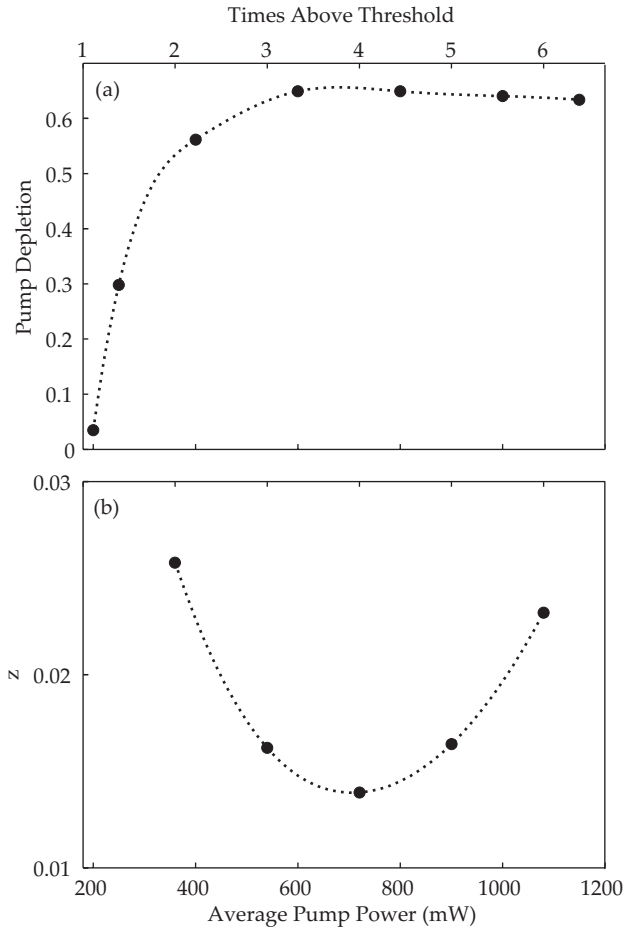

Fig. 7. (a) Pump depletion and (b) spectral transfer fidelity as functions of the average input pump power. The points represent data and the lines are a guide for the eye.

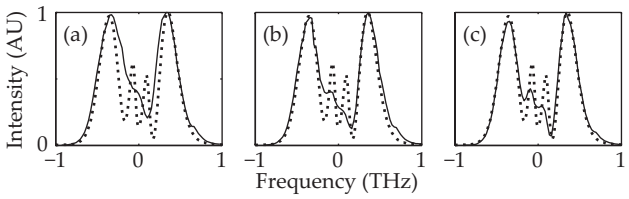

Fig. 8. Measured idler spectra (solid) and input pump spectrum (dashed) for M4 reflectivites of (a) 65%, (b) 85% and (c) 100%.

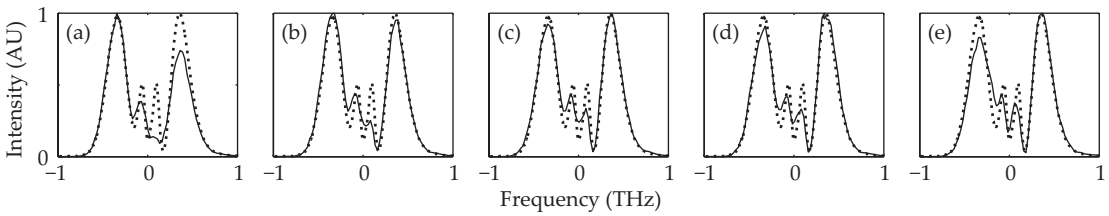

Fig. 9. Measured idler spectra (solid) and input pump spectrum (dashed) for increasing signal delays of (a) -267fs, (b) -133fs, (c) 0fs, (d) +133fs and (e) +267fs in an arrangement where the pump-idler TWO is 48fs.

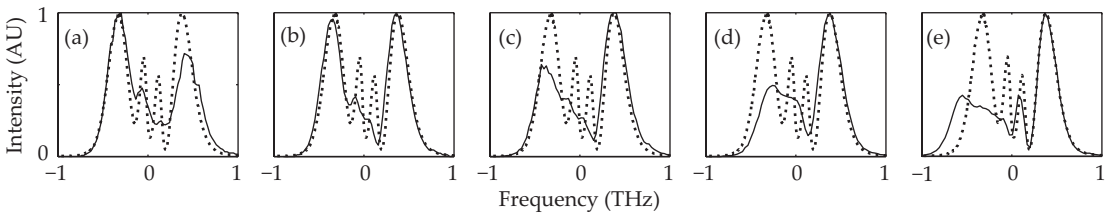

Fig. 10. Measured idler spectra (solid) and input pump spectrum (dashed) for poling periods (a) 29.2μm, (b) 29.5μm, (c) 29.8μm, (d) 30.0μm and (e) 30.2μm showing variation of spectral fidelity as pump-idler TWO varies.

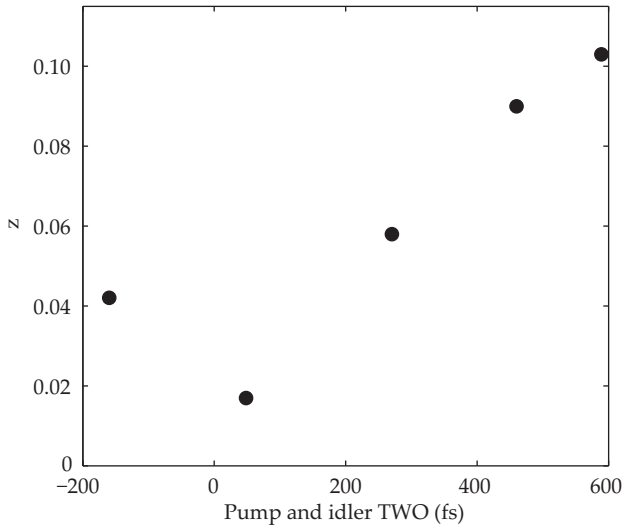

Fig. 11. Spectral fidelity z as a function of pump-idler TWO.

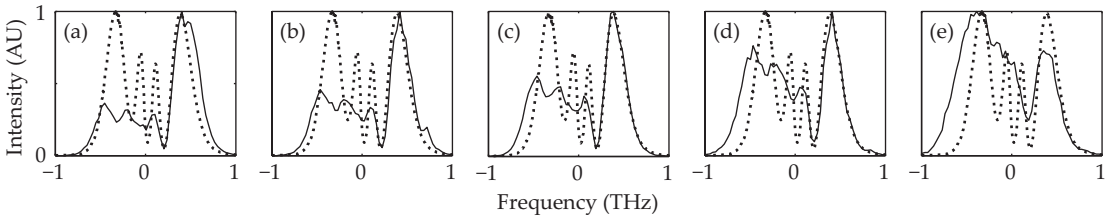

Fig. 12. Measured idler spectra (solid) and input pump spectrum (dashed) for increasing signal delays of (a) -400fs, (b) -133fs, (c) 0um, (d) +266fs and (e) +400fs in an arrangement where the pump-idler TWO is 589fs.

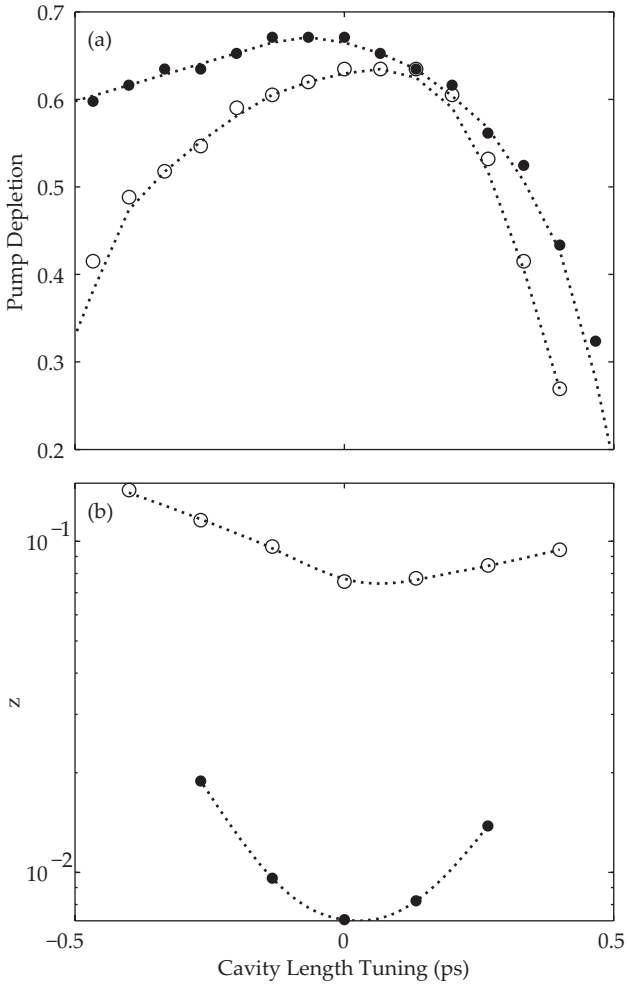

Fig. 13. (a) Pump depletion and (b) fidelity as functions of cavity length for SPOPO arrangements where λ_s=1505 nm (solid circles) and λ_s=1600 nm (open circles). The points represent data and the lines are a guide for the eye.

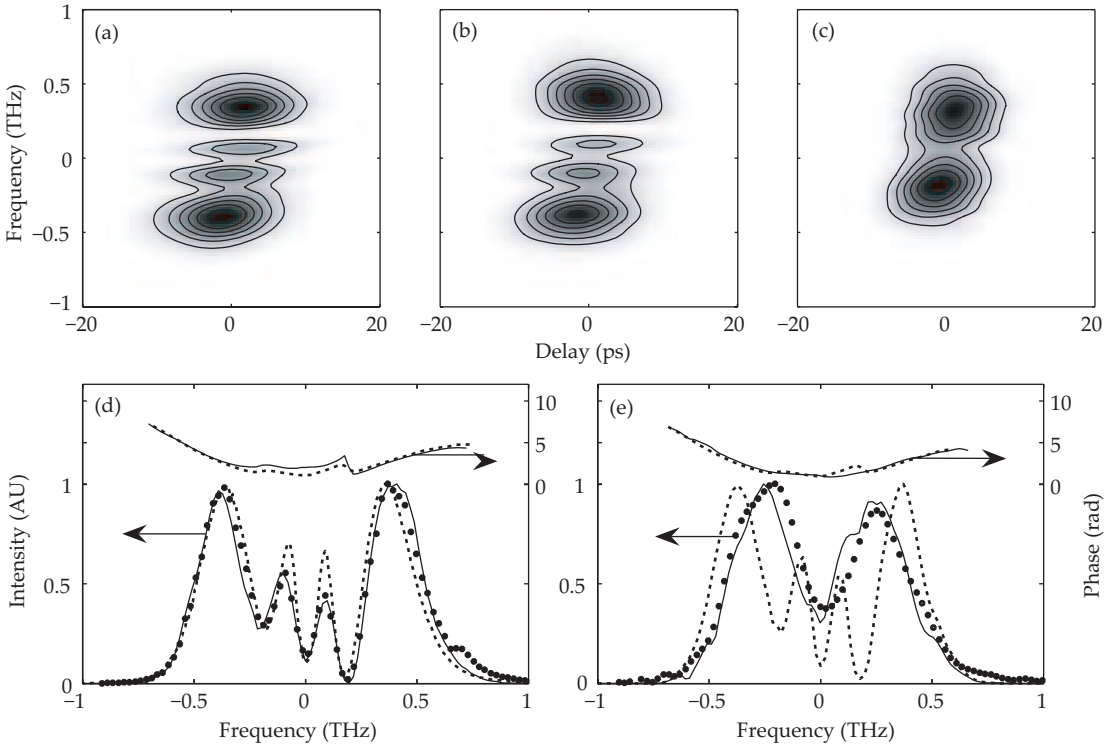

Fig. 14. Demonstration of high fidelity parametric transfer. (a) Retrieved pump sonogram, (b) retrieved idler sonogram for actively preserving parametric transfer and (c) retrieved idler sonogram with no attempts to preserve transfer. (d) and (e) show the retrieved pump spectrum and phase (dashed curve) compared with the measured idler spectrum (circles) and retrieved idler spectrum and phase (solid) for the SPOPO arrangements maintaining and not maintaining high fidelity transfer.